Vol. 7, No. 2, April 2023, pp. 213-221

Current Optics and Photonics

Regular Paper

Thermo-optical Analysis and Correction Method for an Optical Window in Low Temperature and Vacuum

Ruoyan Wang[1], Ruihu Ni[2], Zhishan Gao[1], Lingjie Wang[3], and Qun Yuan[1]*

[1]School of Electronic and Optical Engineering,
Nanjing University of Science and Technology, Nanjing 210094, China
[2]Realsil Microelectronics Inc., Suzhou 215027, China
[3]Changchun Institute of Optics, Fine Mechanics and Physics,
Chinese Academy of Sciences, Changchun 130033, China

(Received October 11, 2022 : revised January 10, 2023 : accepted January 25, 2023)

The optical window, as a part of the collimator system, is the connector between the outside light source and the optical system inside a vacuum tank. The temperature and pressure difference between the two sides of the optical window cause not only thermoelastic deformation, but also refractive-index irregularities. To suppress the influence of these two changes on the performance of the collimator system, thermo-optical analysis is employed. Coefficients that characterize the deformations and refractive-index distributions are derived through finite-element analysis, and then imported into the collimator system using a user-defined surface in ZEMAX. The temperature and pressure difference imposed on the window seriously degrade the system performance of the collimator. A decentered and tilted lens group is designed to correct both field aberrations and the thermal effects of the window. Through lens-interval adjustment of the lens group, the diffraction-limited performance of the collimator can be maintained with a vacuum level of 10^{-5} Pa and inside temperature ranging from −100 ℃ to 20 ℃.

Keywords : Aberration correction, Finite element analysis, Thermoelastic deformation, Thermo-optical analysis

OCIS codes : (000.6850) Thermodynamics; (080.2740) Geometric optical design; (120.6810) Thermal effects; (220.1000) Aberration compensation

I. INTRODUCTION

Large-aperture collimator systems with long focal length are widely used for testing space cameras by providing an infinite objective. Because the actual-use scene of a space camera is a low-temperature vacuum environment, the collimator system should also work in a low-temperature vacuum environment. As an important part of collimator systems, optical windows are employed for light transmission and isolation of pressure and temperature. The temperature and pressure difference between the two sides of the optical window will result in optical-performance degradation of the window. Temperature variations affect the performance of an optical window in two ways: The thermal expansion results in surface deformation, and the temperature variations change the index distribution [1]. Therefore, research on thermo-optical analysis of optical windows and the corresponding correction methods are of great importance when designing an optical system consisting of optical windows.

Numerous thermo-optical analysis methods for optical windows have been reported. One method employed the environmental-analysis option in optical-design software to compensate for the deformation of an optical window [2].

*Corresponding author: karmen86913@gmail.com, ORCID 0000-0003-4561-9723

Color versions of one or more of the figures in this paper are available online.

pISSN: 2508-7266 / eISSN: 2508-7274 https://doi.org/10.3807/COPP.2023.7.2.213

But only the axial temperature field was analyzed in this method, which cannot cover the actual situation. Another method used finite-element software to analyze deformations under the influences of temperature and pressure, with the deformations fitted by Zernike polynomials. The coefficients of the Zernike polynomials were then transferred to optical-design software for further analysis. But this method did not consider the effect of index changes [3, 4]. The third method fitted the refractive index with the formula for gradient index change with temperature and then transferred the fitting coefficients to the optical-design software, but this method did not consider the effect of deformation simultaneously [5]. These methods do not comprehensively analyze the change in the optical system's performance due to optical-window deformation and irregular distribution of refractive index caused by temperature and pressure. To model the thermally induced surface deformation and temperature-dependent refractive index, Bonhoff *et al*. [6] proposed an approach by finite-element analysis (FEA) and ray tracing. However, the aberration-correction method was not given; only spot diagrams were discussed. Furthermore, several correction methods for minimizing thermal effects were reported, including optimizing the window's thickness [7], controlling the window's temperature [8, 9], and designing double-layer window structures [10]. However, those methods cannot compensate for dynamic thermally induced aberrations if the temperature difference between the two sides of the window varies continuously.

In this study the effects of various temperature differences on a window of fused silica are simulated. To solve for the thermal elastic deformation and thermally induced irregular index at the same time, a user-defined surface (UDS) dynamic-link library (DLL) that combines an even aspheric surface and gradient-refractive-index surface is built in the optical-design software ZEMAX. The surface fitting coefficients from FEA are transferred to the written surface, and the wavefront aberration degradation of the overall optical system can be analyzed. To compensate for thermal effects of the optical window, a decentered and tilted lens group is added in front of the window, and measures in response to the change of the temperature difference are also considered.

II. METHOD

2.1. System Design of a Low-temperature Vacuum Collimator

A collimator is taken as an example with the following environment: a low temperature of −100 °C and a vacuum level of 10^{-5} Pa inside, and a normal temperature of 20 °C and normal pressure of 1.01×10^5 Pa outside. The collimator's mechanical structure is illustrated in Fig. 1(a). The focal length of the collimator is 30,000 mm, and its field of view (FOV) is ±40 mm. The effective aperture of the off-axis parabolic mirror is 1,000 mm. The light for this collimator is a quartz tungsten-halogen lamp with a broadband spectrum ranging from 400 to 2,200 nm, which cooperates with narrowband filters centered at different wavelengths depending on the desired test situation. In the optical design and optimization of the collimator system, the working wavelength is set to 550 nm.

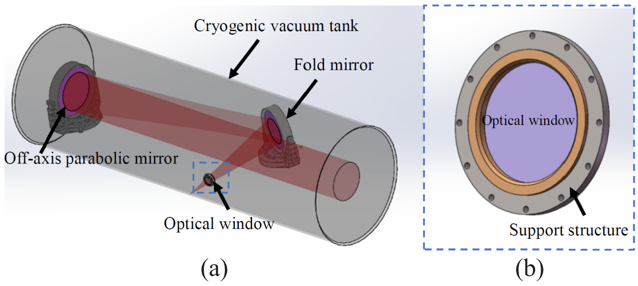

FIG. 1. The mechanical structure of (a) the whole collimator system, and (b) a zoomed-in image of the optical window marked by the blue dashed rectangle in (a).

The collimator consists of three optical elements: An optical window, a flat fold mirror, and an off-axis parabolic mirror. The support structure of optical window is shown in Fig. 1(b). Divergent beams originating from the light source outside pass through the optical window, and then are reflected by the fold mirror and collimated by the off-axis parabolic mirror.

The off-axis parabolic mirror used in this collimator introduces off-axis aberrations, as shown in Fig. 2. As the FOV increases gradually, the wavefront error increases as well. As illustrated in Fig. 2(a), the on-axis aberration can be neglected, while at 0.7 FOV [Fig. 2(b)] the root mean square (RMS) of the wavefront error has exceeded the diffraction limit of the system. At the edge FOV [Fig. 2(c)], the RMS of the wavefront error far exceeds the diffraction limit. The RMS value over the whole FOV is illustrated by the blue trace in Fig. 2(g).

To correct the off-axis wavefront aberration of the collimator originating from the parabolic mirror at room temperature and pressure, a decentered and tilted lens group is placed in front of the optical window, as illustrated in Fig. 3. To ensure the performance of the collimator, the optical power of the compensation lens group is close to zero, and it can be changed by axially displacing the intermediate lens, so there should be at least three components: The front and back ones are fixed, while the intermediate one can be axially displaced. Therefore, the initial configuration of the compensation lens group is selected and added to the initial structure of the collimator system in ZEMAX. The curvature of each lens surface, the intervals between adjacent lenses, decentering values, and tilt angle are selected as variables to optimize the system wavefront error. The optimization is carried out to ensure that the system wavefront error over the full aperture range is below the diffraction limit at room temperature and pressure. The system parameters of the optimized compensation lens group at room temperature and pressure are listed in Table 1. The on-axis

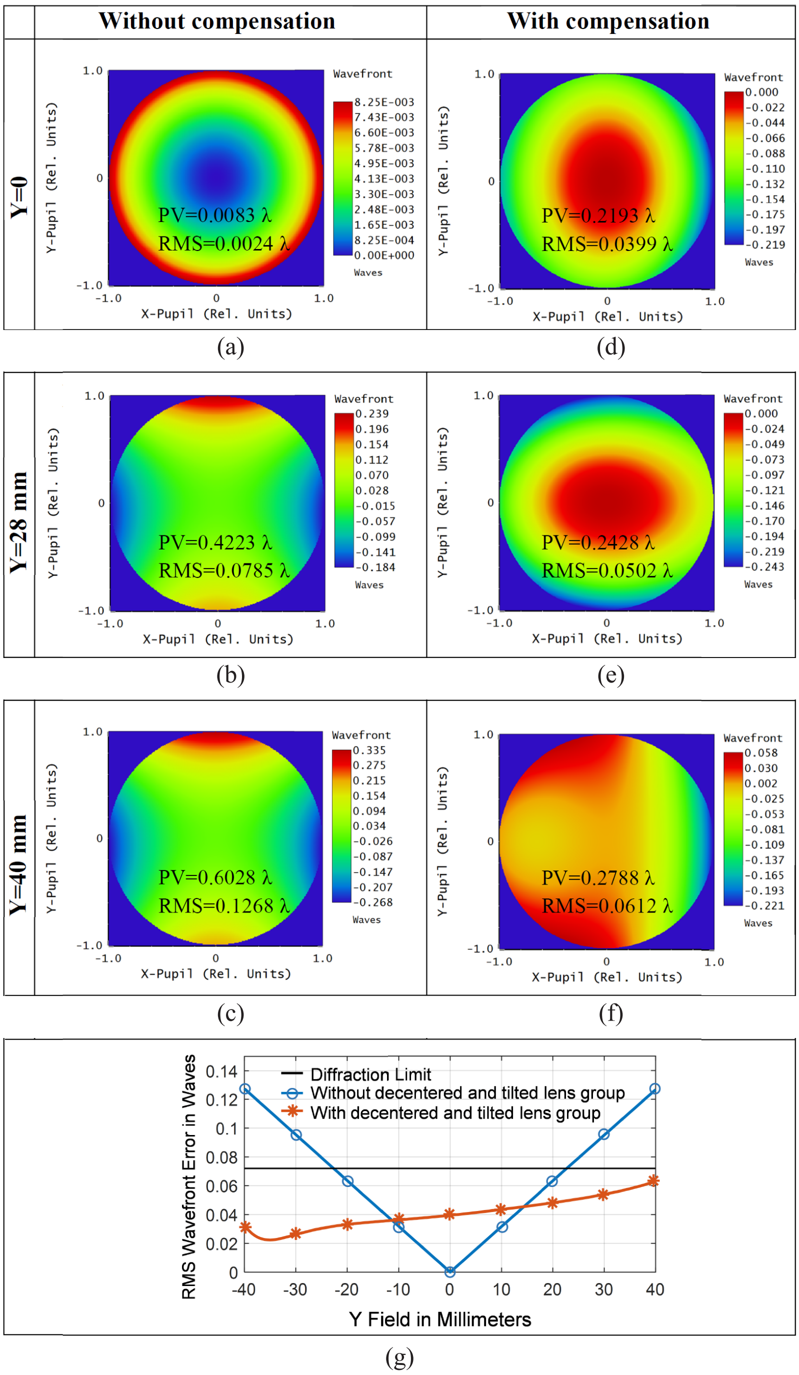

FIG. 2. Wavefront aberrations of the collimator, before (a)–(c) and after (d)–(f) placing a decentered and tilted lens group. (g) shows the RMS wavefront-aberration versus FOV curves with and without the compensation lens group. RMS, root mean square; FOV, field of view.

and off-axis wavefront errors are shown in Figs. 2(d)–2(f). After employing the compensation lens group, off-axis aberrations are well suppressed. The orange RMS wavefront error versus FOV curve plotted in Fig. 2(g) indicates that the wavefront aberration decreases below the diffraction limit across the full FOV, after employing the decentered and tilted lens group.

2.2. Thermo-optical Analysis of the Optical Window

As an important part of the collimator, the optical window connects the external light source and the optical system in the vacuum tank. The temperature and pressure difference between the two sides of the optical window not only cause thermoelastic deformation, but also introduce an irregular distribution of the refractive index of the whole window. To show the effects of these two changes on the performance of the collimator, thermo-optical analysis of the optical window should be conducted.

An optical window with aperture of Φ200 mm and thickness of 30 mm is placed in a circular, rigid support frame. The support frame is fixed to the cryogenic vacuum tank, and the periphery of the window is pressed with a copper coil.

Since the temperature difference between the two sides of the optical window is very large, fused silica and 304 steel are selected as the materials for window and support structure respectively, due to their small thermal expansion coefficients. The material for the pressing ring is copper. The characteristic parameters of these materials are listed in Table 2.

The model for the optical window is established in SolidWorks, and its temperature distribution can be obtained using FEA software. The parameters of the materials, temperature loads with 20 °C outside and −100 °C inside, and the boundary conditions for each part are added in the software. A thermal analysis of the optical window is conducted using the conditions mentioned above. The temperature distribution of the optical window is shown in Fig. 4.

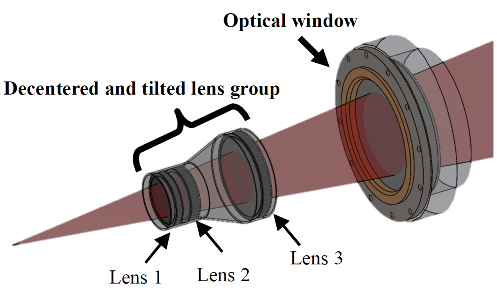

FIG. 3. The mechanical structure of the decentered and tilted lens group.

2.2.1. Analysis of Thermally Induced Index Irregularities

The refractive index is temperature dependent, and the change in refractive index of a lens with temperature variation is given by [11]

$$\Delta n = \frac{n_0^2 - 1}{2n_0^2}[D_0\Delta T + D_1\Delta T^2 + D_2\Delta T^3 + \frac{E_0\Delta T + E_1\Delta T^2}{\lambda^2 - \lambda_{tk}{}^2}], \tag{1}$$

where Δn represents the change in refractive index, n_0 represents the refractive index of the lens at reference temperature, which is usually 20 °C , with respect to the refrac-

TABLE 1. Parameters of the decentered and tilted lens group

Parameter	Lens 1	Lens 2	Lens 3
R1 (mm)	135.138	673.712	−220.180
R2 (mm)	130.440	−1446.631	−514.718
Thickness (mm)	20	20	25
Material	Fused Silica	Fused Silica	Fused Silica
Interval (mm)	23.455	106.545	281.535
Decentering Value (mm)	24.663	24.663	24.663
Tilt (deg)	−7.476	−7.476	−7.476

TABLE 2. Properties of the materials used in the thermal analysis

Material	Elasticity modulus (GPa)	Density (kg/m^3)	Poisson's ratio υ	Thermal expansion coefficient (ppm/°C)	Thermal conductivity (J/kg·K)
Fused Silica	117	2250	0.17	0.58	1.4
304 Steel	193	8000	0.27	14.7	16.2
Copper	73	8940	0.34	16.9	391

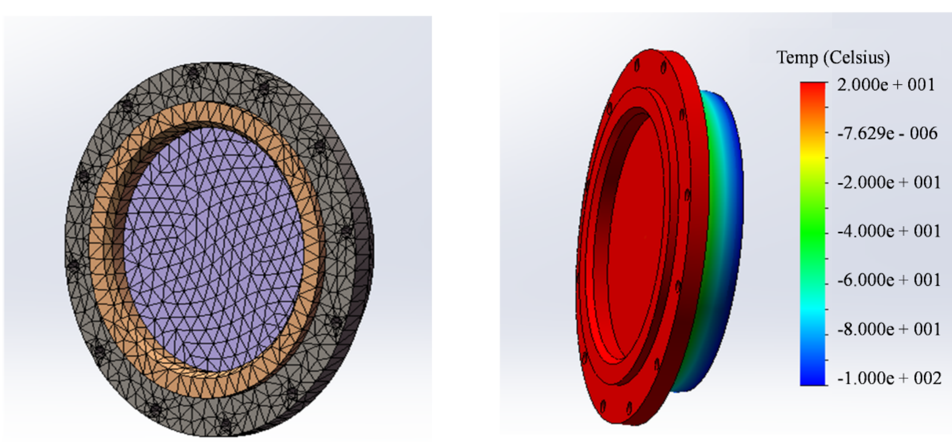

(a) (b)

FIG. 4. Results of finite-element analysis of the optical window: (a) window after meshing, and (b) temperature distribution of the optical window with 20 °C outside and −100 °C inside.

tive index of air, ΔT represents the temperature change of the lens with respect to the reference temperature, λ is the wavelength, and D_0, D_1, D_2, E_0, E_1, and λ_{tk} are the thermal index constants related to the materials.

The temperature of each node of the window is obtained from the thermal analysis. The value of refractive-index change corresponding to the temperature differences of all the nodes is quantitatively calculated using Eq. (1). Table 3 lists the change in refractive index for some nodes (in which the z direction represents the optical axis).

The GRIN surface is used to characterize a gradient index surface in ZEMAX. The GRIN 4 surface model is described as [12]

$$\Delta n = n - n_0 = n_{x1}x + n_{x2}x^2 + n_{y1}y + n_{y2}y^2 + n_{z1}z + n_{z2}z^2. \quad (2)$$

Due to the rotational symmetry of the temperature loads, the irregularities in refractive index are fitted with a rotationally symmetrical gradient index. The coefficients satisfy $n_{x1} = n_{y1} = 0$ and $n_{x2} = n_{y2}$, so the refractive index of the gradient index surface is defined as

$$\Delta n = n - n_0 = n_{r2}r^2 + n_{z1}z + n_{z2}z^2, \quad (3)$$

where $r^2 = x^2 + y^2$, n_0 represents the substrate's refractive index, n_{r2} represents the radial index coefficient, and n_{z1} and n_{z2} represent the index coefficients along the z direction.

For all nodes, the index changes are

$$\begin{cases} \Delta n_1 = n_{r2}r_1^2 + n_{z1}z_1 + n_{z2}z_1^2 \\ \Delta n_2 = n_{r2}r_2^2 + n_{z1}z_2 + n_{z2}z_2^2 \\ \ldots\ldots \\ \Delta n_t = n_{r2}r_t^2 + n_{z1}z_t + n_{z2}z_t^2 \end{cases}. \quad (4)$$

This can be written in matrix form as:

$$\mathbf{AX} = \mathbf{Y}, \quad (5)$$

where $\mathbf{A} = \begin{bmatrix} r_1^2 & z_1 & z_1^2 \\ r_2^2 & z_2 & z_2^2 \\ \cdots & \cdots & \cdots \\ r_t^2 & z_t & z_t^2 \end{bmatrix}$, $\mathbf{X} = \begin{bmatrix} n_{r2} \\ n_{z1} \\ n_{z2} \end{bmatrix}$, and $\mathbf{Y} = \begin{bmatrix} \Delta n_1 \\ \Delta n_2 \\ \vdots \\ \Delta n_t \end{bmatrix}$.

The coefficients vector **X** of Eq. (5) can be determined using the least-squares method. n_{r2}, n_{z1}, n_{z2} are the gradient refractive index coefficients of the optical window at the corresponding temperature difference, and they are imported into the UDS. For environments with various temperature differences, the coefficients are listed in Table 4.

2.2.2. Analysis of Deformation Caused by Temperature and Pressure Difference

The deformation of the window can be analyzed by finite-element mechanical analysis. The temperature and pressure loads are applied to the optical window, and appropriate fixing is added to the support structure. After grid division of the whole window and supporting structure, thermo-optical analysis is carried out to obtain the deformations of the optical window caused by different temperature differences. When the temperature inside the vacuum tank is −100 °C and the pressure is 10^{-5} Pa, and the temperature outside the tank is 20 °C and the pressure is a standard atmosphere (1.01 × 10^5 Pa), the deformation of the optical window is shown in Fig. 5.

An even-order aspherical surface is used to fit the rotationally symmetric deformation:

$$z = \sum_{i=1}^{8} \alpha_i \cdot r^{2i}, \quad (6)$$

where the α_i represent the even aspheric coefficients. The coefficients of the outside and inside surfaces after the fitting process are shown in Table 5. The even aspheric terms

TABLE 4. Index coefficients of the optical window for various temperature differences

ΔT (°C)	n_0	n_{r2} (mm^{-2})	n_{z1} (mm^{-1})	n_{z2} (mm^{-2})
−20	1.458464	−5.896E-11	−5.639E-06	5.199E-09
−40	1.458464	−1.206E-10	−1.129E-05	1.973E-08
−60	1.458464	−1.750E-10	−1.695E-05	4.426E-08
−80	1.458464	−2.240E-10	−2.263E-05	7.952E-08
−100	1.458464	−2.666E-10	−2.834E-05	1.262E-07
−120	1.458464	−3.017E-10	−3.408E-05	1.851E-07

TABLE 3. Change in refractive index for some nodes

Node	Coordinate x (mm)	Coordinate y (mm)	Coordinate z (mm)	ΔT (°C)	Index difference Δn (*1E-4)
1	−15.0293	−21.4224	0	0	0
2	4.2003	3.6109	1.6157	−6.50	−0.544
3	95.1811	−6.4238	2.8779	−11.58	−0.964
4	74.5497	−12.9755	5.1408	−25.83	−2.110
5	−62.9733	−35.0015	12.0235	−48.10	−3.820
6	−39.5141	−94.5852	16.5170	−66.50	−5.160
7	−2.9773	47.2227	20.8290	−83.30	−6.300

r^{12}, r^{14}, and r^{16} may be ignored because their influences on the surface are minor. The deformations of the inside and outside surfaces of the window under various temperature differences are presented as the surface sag across the diameter of the window, in Figs. 6(a) and 6(b) respectively [13].

Taking the analysis in Sections 2.2.1 and 2.2.2 into consideration comprehensively, a UDS is inserted in ZEMAX for the combination of the gradient index surface and even aspherical surface. The gradient index coefficients and the even aspherical surface coefficients are compiled into a DLL file. For different temperature nodes, the corresponding surface DLL file is selected for further evaluation of system performance.

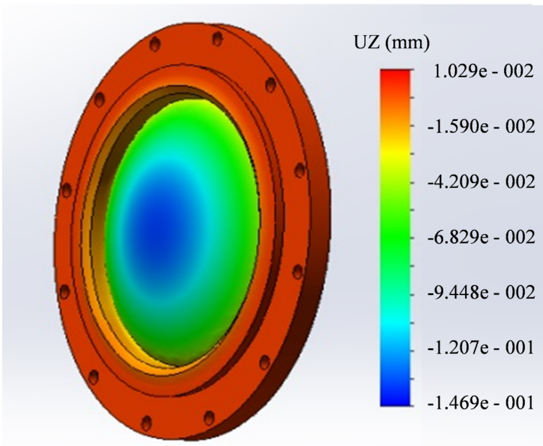

FIG. 5. The optical window's thermal deformation, with 20 °C outside and −100 °C inside.

2.3. Optical-performance Evaluation and Correction Method

2.3.1. Dynamic Correction of Thermal Effect in Low-temperature and Vacuum Environment

According to the thermal-deformation analysis of the optical window in Section 2.2, with increasing temperature and pressure difference between the inside and outside of the window, the surface shape and refractive-index distribution of the window change, which has an impact on the wavefront aberration of the system. Even though the off-axis aberrations at room temperature and pressure have been corrected with the compensation lens group described in Section 2.1, the wavefront aberration of the collimator exceeds the diffraction limit again as the temperature difference increases. The effects due to temperature differences of −80 °C and −120 °C are presented in Fig. 7, illustrated by dark orange and blue lines respectively. As the temperature difference increases, the system wavefront aberrations of some fields are above the diffraction limit, even with the decentered and titled lens group, and for most of the FOV, the larger the temperature difference, the larger the wavefront aberration.

TABLE 5. Surface coefficients of the optical window for various temperature differences

ΔT (°C)	Outside Surface					Inside Surface				
	α_1 ($\times 10^{-5}$ mm^{-2})	α_2 ($\times 10^{-10}$ mm^{-4})	α_3 ($\times 10^{-14}$ mm^{-6})	α_4 ($\times 10^{-21}$ mm^{-8})	α_5 ($\times 10^{-25}$ mm^{-10})	α_1 ($\times 10^{-5}$ mm^{-2})	α_2 ($\times 10^{-10}$ mm^{-4})	α_3 ($\times 10^{-14}$ mm^{-6})	α_4 ($\times 10^{-21}$ mm^{-8})	α_5 ($\times 10^{-25}$ mm^{-10})
−20	0.1518	−1.044	1.091	1.613	−2.939	0.1298	0.2454	−0.2241	3.833	−4.074
−40	0.3297	−1.327	1.286	−2.543	2.515	0.2884	0.5086	−0.4574	9.339	−9.894
−60	0.5046	−2.173	2.037	1.841	3.578	0.434	0.7614	−0.6885	−1.305	−1.552
−80	0.6742	−2.92	2.73	3.932	4.688	0.58	1.246	−1.083	−1.505	−2.214
−100	0.8411	−3.588	3.373	2.545	6.029	0.7274	1.521	−1.335	−1.239	−2.793
−120	1.007	−4.259	4.022	5.014	7.236	0.871	1.868	−1.626	−2.373	−3.306

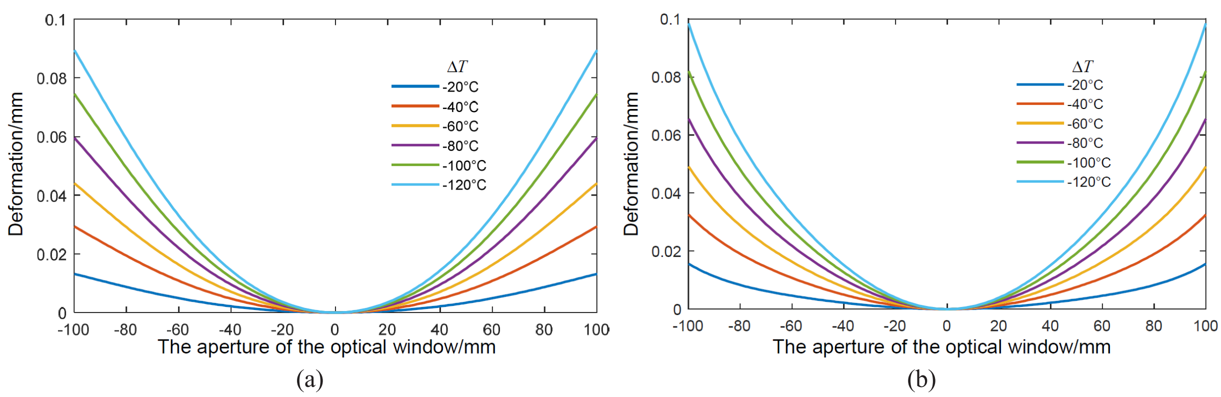

FIG. 6. The deformation of the silica window's (a) outside surface and (b) inside surface, for different temperature differences.

With increasing temperature difference, the wavefront aberration of the system also changes dynamically and gradually exceeds the diffraction limit of the system, affecting the output beam quality of the system. Therefore, a corresponding compensation method is applied with focus shift of the decentered and tilted lens group, which is realized by lens-interval adjustment of the lens group, to obtain a zoomed compensation lens.

As shown in Fig. 8, the position of the intermediate lens of the group is adjustable, to restrain the wavefront error according to the temperature difference.

2.3.2. Process of Thermal Analysis and Dynamic Correction of Thermal Effects

The flowchart of the thermo-optical analysis and correction process for the optical window is illustrated in Fig. 9. It takes both thermally induced deformation and thermally induced index irregularities into consideration.

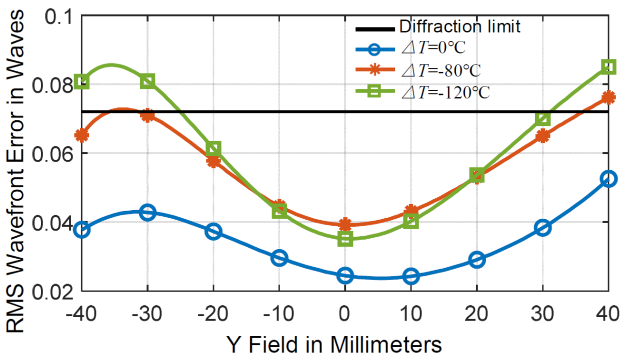

FIG. 7. RMS wavefront aberration VS FOV under different temperature difference. RMS, root mean square; FOV, field of view.

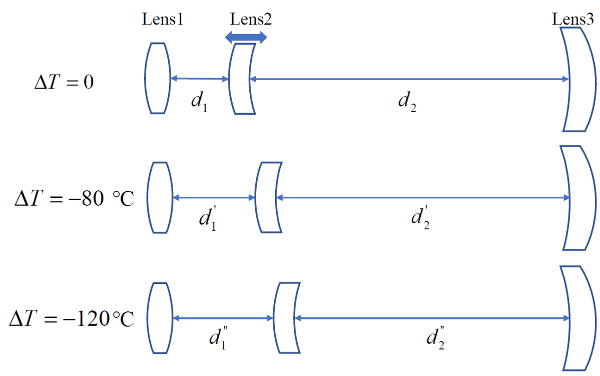

FIG. 8. Schematic diagram of the compensation lens group under various temperature differences.

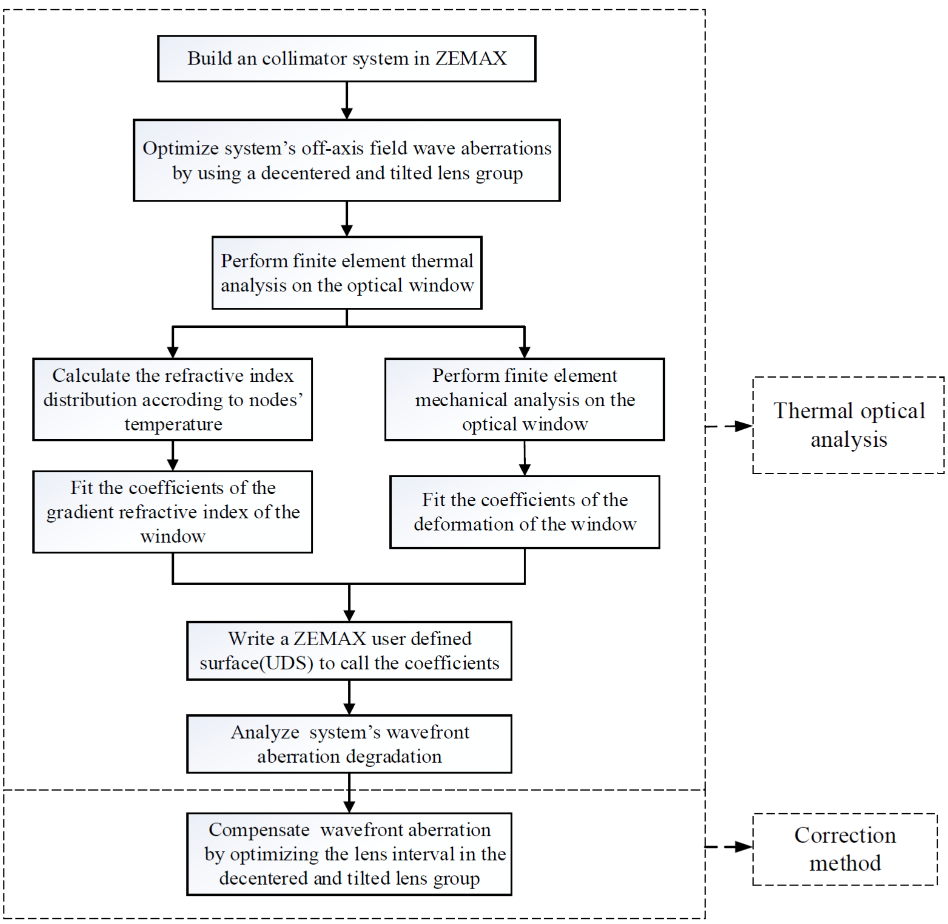

FIG. 9. The process of thermo-optical analysis and correction for the optical window.

TABLE 6. Lens intervals for different temperature differences

ΔT (°C)	0	−20	−40	−60	−80	−100	−120
d_1 (mm)	23.455	23.696	23.967	24.385	24.697	24.972	25.286
d_2 (mm)	106.545	106.304	106.033	105.615	105.303	105.028	104.714

The processes are as follows: (1) Build a collimator system in ZEMAX. and correct its off-axis field wavefront aberration using a decentered and tilted lens group. (2) Create the model of the optical window in SolidWorks, and perform finite-element thermal analysis to obtain the temperature distribution of the window. (3) Fit the coefficients of the gradient refractive index of the window according to node temperatures. (4) Add pressure and temperature loads to perform finite-element mechanical analysis, and fit the coefficients of the deformation of the surface. (5) Write the UDS file to call the refractive-index and surface coefficients in ZEMAX. (6) Analyze system optical performance under low temperature and vacuum environment. (7) Optimize the lens interval in the decentered and tilted lens group to compensate for the wavefront aberration degradation, getting a zoomed compensation lens group.

2.3.3. Results of Correction of Thermal Effects at Different Temperature Differences

Based on the above idea, multiple configurations are employed to represent the collimator system under different temperature differences. The interval d_1 between Lens 1 and Lens 2 is set as a variable, and the interval d_2 between Lens 2 and Lens 3 is set to guarantee $d_1 + d_2 = 130$ mm. Wavefront error is still selected as the evaluation function, for the seven temperature nodes chosen in this paper, and the optimization results for the intervals between the three lenses are shown in Table 6. As the temperature difference increases, the interval between Lens 1 and Lens 2 gradually increases.

The RMS aberration versus FOV after correction is plotted in the solid lines in Figs. 10(a) and 10(b), for ΔT of −80 °C and −120 °C respectively. Within the whole FOV, the wavefront aberrations of the system are below the system's diffraction limit. This verifies that the zoom compensation lens group not only can correct the aberration caused by the off-axis parabolic mirror, but also can dynamically correct the thermal effects caused by different temperature and pressure differences, to ensure system performance.

The overall assembly structure is employed in the compensation lens group. Lens 1 and Lens 3 are fixed by pressure rings, while Lens 2 is placed in a threaded mount. Thermally induced aberrations are dynamically corrected by rotating the recessed collar on the barrel of the lens. The tolerances are carefully considered to guarantee output beam quality. The tolerances are 0.1 mm for decentering and 2′ for tilt angle, which are easy to meet with a high-precision adjustment mechanism.

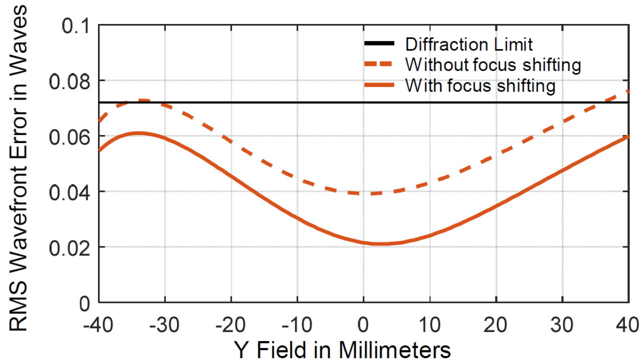

(a)

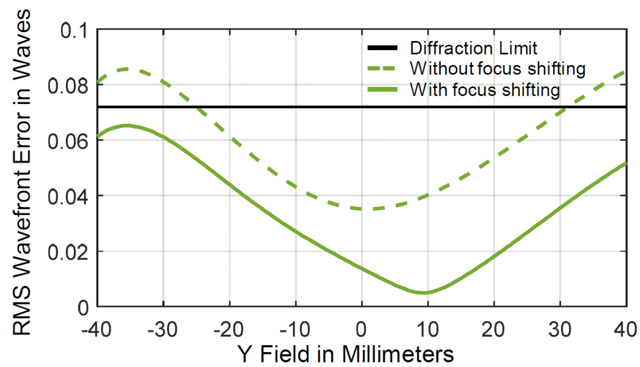

(b)

FIG. 10. RMS wavefront aberration versus FOV. (a) ΔT is −80 °C, without (dotted line) and with (solid line) focus shifting. (b) ΔT is −120 °C, without (dotted line) and with (solid line) focus shifting. RMS, root mean square; FOV, field of view.

III. CONCLUSION

Based on the UDS of the optical design software ZEMAX, thermo-optical analysis of the fused-silica window of a collimator was performed to obtain the influences of the window's deformations and index irregularities under various temperature differences. Using the UDS, the refractive index and surface deformation are successfully determined in the thermal analysis. The changes of the window under vacuum and low temperature affect the system wavefront aberration. By designing a decentered and tilted lens group, the field aberrations originating from the off-axis parabolic mirror were decreased. Through lens-interval adjustment of the lens group at each operating temperature, the wavefront aberration caused by thermal effects was minimized below the diffraction limit. This paper provides a solution for the thermo-optical analysis of an optical window, and a compensation method for a collimator system with an optical window.

FUNDING

National Key Research and Development Program (2019YFB2005500); National Natural Science Foundation of China (62205148, 62175107, U1931120); Six talent peaks project in Jiangsu Province (RJFW-019); Foundation of key laboratory of optical system advanced manufacturing technology, Chinese academy of sciences (KLOMT190201); Foundation of Shanghai key laboratory of online test and control technology (ZX2021102).

DISCLOSURES

The authors declare no conflicts of interest.

DATA AVAILABILITY

Data underlying the results presented in this paper are not publicly available at the time of publication, but may be obtained from the authors upon reasonable request.

REFERENCES

1. K. B. Doyle, V. L. Genberg, and G. J. Michels, *Integrated optomechanical analysis*, 2nd ed. (SPIE, Washington, USA, 2012).
2. K. B. Doyle and J. M. Hoffman, “A thermal design and analysis for WDM applications,” Proc. SPIE **4444**, 130–140 (2001).
3. G. Zhang, H. Yang, C. Mei, K. Shi, D. Wu, and M. Qiao, “Thermal structural optical integrated design for optical window of a high-speed aerial optical camera,” Proc. SPIE **9676**, 96760W (2015).
4. E. Flamini, E. Segato, V. Da Deppo, S. Debei, G. Naletto, G. Cremonese, and E. Flamini, “Method for studying the effects of thermal deformations on optical systems for space application,” Appl. Opt. **50**, 2836-2845 (2011).
5. X. Song, L. Li, and Y. Huang, “Method of determining effects of heat-induced irregular refractive index on an optical system,” Appl. Opt. **54**, 7701–7707 (2015).
6. T. Bonhoff, L. Busing, J. Stollenwerk, and P. Loosen, “Modeling of optical aberrations due to thermal deformation using finite element analysis and ray-tracing,” Proc. SPIE **9626**, 96261V (2015).
7. M. Li, Q. Wu, and F. Yu, “Optimization of optical window glass thickness based on the thermal optical analysis,” Acta Optica Sinica **30**, 210 (2010).
8. B. Bohannan, E. T. Pearson, and D. Hagelbarger, “Thermal control of classical astronomical primary mirrors,” Proc. SPIE **4003**, 406–416 (2000).
9. A. Miyashita, R. Ogasawara, G. Macaraya, and N. Itoh, “Temperature control for the primary mirror of Subaru Telescope using the data from ‘forecast for Mauna Kea observatories’,” Publ. Natl. Astron. Obs. Japan **7**, 25-31 (2003).
10. Y. Xu, N. Wang, and Y. Xu, “Design analysis of double optical window of high speed aerial remote sensor,” Acta Optica Sinica **35**, 0122007 (2015).
11. M. Englert, P. Hartmann, and S. Reichel, “Optical glass: Refractive index change with wavelength and temperature,” Proc. SPIE **9131**, 91310H (2014).
12. Zemax LLC, “OpticStudio,” (Zemax LLC), http://www.zemax.com/ (Accessed Date: Sep. **16**, 2022).
13. P. A. Coronato and R. C. Juergens, “Transferring FEA results to optics codes with Zernikes: A review of techniques,” Proc. SPIE **5176**, 1–8 (2003).